

An experimental and modeling investigation of particle production by spray pyrolysis using a laminar flow aerosol reactor

I. Wuled Lenggoro, Takeshi Hata, and Ferry Iskandar

Department of Chemical Engineering, Hiroshima University, Kagamiyama 1-4-1, Higashi-Hiroshima 739-8527 Japan

Melissa M. Lunden

Environmental Energy Technologies Division, Lawrence Berkeley National Laboratory, 1 Cyclotron Road, Berkeley, California 94720

Kikuo Okuyama^{a)}

Department of Chemical Engineering, Hiroshima University, Kagamiyama 1-4-1, Higashi-Hiroshima 739-8527 Japan

(Received 21 July 1999; accepted 28 December 1999)

The influence of operating parameters on the morphology of particles prepared by spray pyrolysis was investigated using a temperature-graded laminar flow aerosol reactor. Experimentally, zirconia particles were prepared by spray pyrolysis using an aqueous solution of zirconyl hydroxide chloride. Hollow particles were formed if the reactor temperature was high, the temperature gradient was too large, the flow rate of carrier gas was high, and the initial solute concentration was low. A numerical simulation of the pyrolysis process was developed using a combination of two previous models. The simulation results compared well with the experimental results.

I. INTRODUCTION

Small particles with sizes of submicron up to several micrometers have important applications in the areas of electronic materials, catalysis, and analytical chemistry. It is important to develop a process which can produce the particles having controlled characteristics such as size, morphology, composition, and others. To be industrially relevant, the process needs to be low cost with both a continuous operation and a high production rate. Spray pyrolysis, a method for producing particulate materials that combines both liquid and gas phase aerosol processes, may be such a process.¹

Particle synthesis by spray pyrolysis involves the atomization of a precursor solution into discrete droplets. These droplets are subsequently transported through a furnace where the solvent is evaporated from the droplets and the dissolved species react to form the product particulate. Spray pyrolysis has a number of advantages including the following: (i) the particles produced are spherical; (ii) the distribution of their diameters is uniform and controllable from micrometer to submicron; (iii) the purity of the product is high; (iv) the process is

continuous. These advantages are realized because the precursor salts are mixed in solution at the molecular level; after atomization, all particle formation processes are integrated inside the droplet. Each droplet has the same composition; thus multicomponent and composite particles can be easily synthesized by controlling the chemistry of the precursor solution. The application of the spray pyrolysis process to industry is very promising because the equipment is simple with short processing times on the order of a few seconds. By comparison, the use of conventional solid-phase or liquid-phase methods requires the repetition of some operations, such as calcination and milling, to obtain the desired particle size. Moreover, these operations often introduce impurities into the particles.

Using the spray-pyrolysis method, our group has been preparing various functional fine particles such as metal oxide superconductors,² metal sulfides,^{3,4} and recently some oxide phosphors.⁵ In these papers, the relationships between physical properties of the prepared particles like morphology and the process conditions have been experimentally investigated.

Much of the work regarding spray pyrolysis had focused on the prediction and control of the final particle morphology. A number of investigators have reported on numerical solutions of the droplet-to-particle conversion

^{a)}Address all correspondence to this author.
e-mail: okuyama@ipc.hiroshima-u.ac.jp

process. Marshall and colleagues^{6–12} investigated the effect of solvent evaporation rate on the morphology of dried particles by deriving the diffusion equation for the mass transfer of a dissolved solid inside a droplet. The diffusion equations presented in Marshall's paper^{6,7} were too complicated to be solved analytically due to the moving boundary caused by the shrinkage of the droplet. Thus, this initial work on mass transfer inside a droplet employed several assumptions, which limited the use of the solutions. The difficulty involved in the calculation of the moving boundary problem was greatly simplified by van der Lijn¹³ by proposing a mathematical relation for fixing the outer boundary. This technique enables a simple analytical relation for calculating the solute concentration distribution inside a droplet.

Most of these earlier studies were qualitative in nature and usually examined relatively large particles of size 100 to 1000 μm . Among the few studies for droplets of size 10 to 100 μm , Leong⁹ proposed that limited control of particle morphology could be achieved by controlling the temperature and humidity of the carrier gas as well as the precursor solution characteristics.

Jayanthi *et al.*¹¹ applied van der Lijn's technique¹² to solve the diffusion equation inside the droplet to model the evaporation and solute precipitation of 10- μm zirconia particles. They assumed that homogeneous nucleation would occur when the solute concentration at the surface of the droplet reached the critical supersaturation. After nucleation of the solid, precipitation occurs only in the part of the droplet where the solute concentration is higher than the equilibrium saturation. Hollow particles result if the solute concentration at the center of the droplet is less than the equilibrium saturation of the solute. Using their model, they predicted the morphology resulting from the spray pyrolysis of ZrO_2 from zirconyl hydroxide chloride, a precursor for which they had previously measured the values of the critical and equilibrium saturations.¹⁴ Their calculations considered the effects of parameters such as process temperature and the initial solute concentration on the morphology of single particles. They found that lower process temperatures and higher initial solute concentrations favored the formation of dense particles.

Of all the numerical studies of the droplet to particle conversion process, only one considered the effect of multiple droplets.¹² Their calculations were performed using sodium chloride as a model compound. They presented calculation results for the change of solvent vapor concentration, droplet size, and droplet temperature during heating in a laminar flow reactor by varying values like the initial number concentration of ambient humidity. However, their model did not consider the change of mass concentration inside the droplets due to evaporation. All droplets were assumed to form solid, dense particles; no attempt was made to model particle mor-

phology. Moreover, neither their modeling results nor the results of Jayanthi *et al.* are directly compared with experimental results.

Clearly, the formation of particles by spray pyrolysis is a complex process and is difficult to accurately model. The task is made more difficult by the lack of data on the chemistry and solubility of many precursors, as well as nucleation and crystallization during precipitation. It is essential to develop a model that considers both multiple droplets and changes in mass concentration within the droplets. Until now, this important problem has been left unsolved.

In this study, we present a model of the particle formation process that is based on the models presented by Jayanthi *et al.*¹¹ and Xiong and Kodas.¹² Our model simultaneously computes the evaporation rate from a monodisperse population of aerosol particles and the change of the solute concentration within the droplets. The change in droplet size and particle morphology is calculated as a function of position in the reactor and process time. For experimental comparison, zirconia particles were prepared using the spray-pyrolysis process at a number of operating conditions. Zirconia was selected because of its wide application in industry due to its outstanding mechanical strength, thermal stability, chemical resistance, and electrical characteristics. In addition, values of the material-property data required for the modeling study are available in the literature.¹¹

II. EXPERIMENTAL PROCEDURE

A schematic of the experimental apparatus used to produce and collect the zirconia particles is shown in Fig. 1. The main equipment consists of (i) a nebulizer that converts the starting solution into microdroplets, (ii) the carrier gas, (iii) a tubular, laminar flow aerosol reactor, and (iv) a sampler or precipitator. The starting solution was atomized at a frequency of 1.75 MHz by an ultrasonic nebulizer (Omron Co., Kyoto, Japan, Model NE-U11B), which was cooled with running water. The level of the spray solution was kept constant to ensure a uniform generation rate of droplets. Figure 2 shows the equivalent volume diameter distribution of the atomized water droplets as measured by a light-scattering particle-size analyzer (Malvern Instruments Corp., Worcester-shire, U.K., Mastersizer DPF). The average equivalent volume diameter of solution droplets was 4.5 μm . Water was used as the solvent. The tubular furnace was an alumina tube of 13-mm inside diameter and about 1000 mm long. The furnace consists of five independently controlled heating zones, each 200 mm in length, enabling flexibility in the production of the experimental temperature distributions. The temperature of each heating zone was controlled to within 2 °C. A pre-

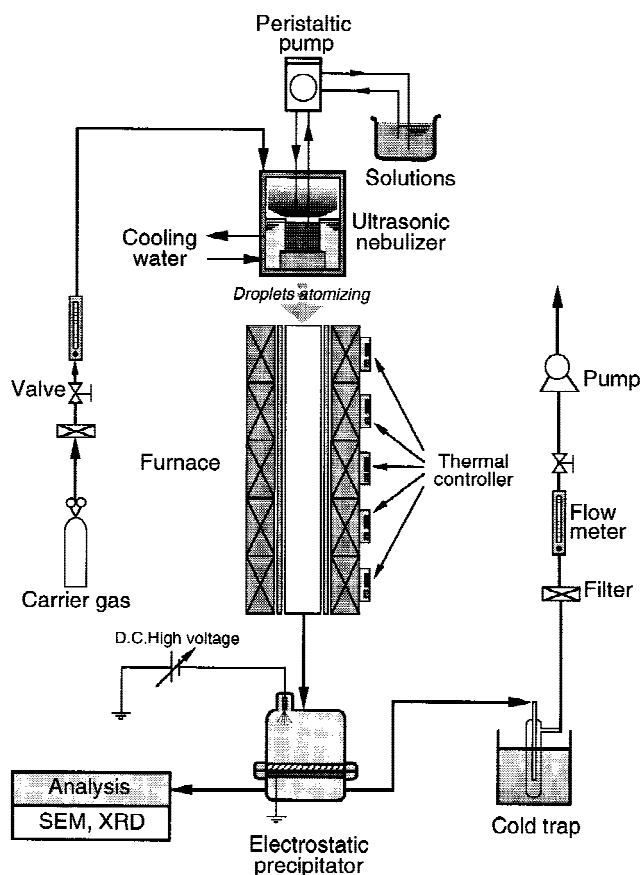


FIG. 1. Experimental apparatus.

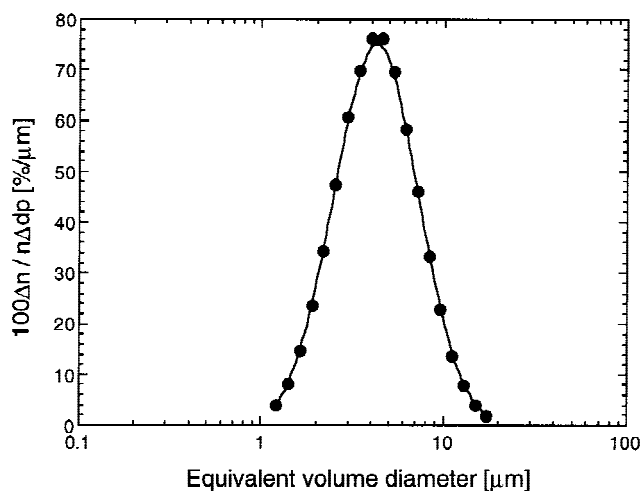


FIG. 2. Size distribution of aqueous droplets using an ultrasonic nebulizer.

vious numerical evaluation of the reactor¹⁵ showed that the flow in the reactor is laminar for gas flow rates between 0.5 to 2 l/min. The Reynolds numbers of all conditions performing in present study are less than 200. The carrier gas used was nitrogen or air. Laminar flow is necessary for comparison with the results of the numerical simulations.

A zirconium hydroxide chloride ($\text{ZrO}(\text{OH})\text{Cl}$) solution (Nikkei-MEL, Japan-U.S.A.) was used as the precursor for producing ZrO_2 particles. All experiments were performed using a molar concentration of 2.0 mol/l. The physical properties of this solution are shown in Table I.

III. NUMERICAL PROCEDURE: PHYSICAL MODEL AND BASIC EQUATIONS

A schematic of the droplet evaporation and precipitation process is shown in Fig. 3. The model of this process describes both the change of droplet diameter and the particle morphology by simultaneously considering the evaporation of multiple droplets along a tubular aerosol reactor and the concurrent solute concentration distribution within the droplet. Monodispersed droplets having diameter $2R_{p0}$, number concentration N_0 , and solution concentration C_0 are introduced into the reactor with relative humidity RH^0 and ambient temperature T_0 , flowing in either air or nitrogen at flow rate Q . The reactor has length L and an inner diameter of $2R$. The reactor wall is maintained at a temperature T_w . During solvent evaporation, the size of the droplets decreases and the solution concentration inside each droplet increases as the aerosol travels through the reactor. Eventually, the solute concentration inside the droplet reaches the critical supersaturation ratio at which point solute nucleation, precipitation, decomposition, and other solid-state processes take place within the particle.

Figure 4 shows a schematic of how the solute concentration within the droplet changes during solvent evaporation, based on the formalism proposed by Jayanthi *et al.*¹¹ The graphs in Fig. 4 show how the solute concentration varies inside the droplet. The horizontal axis represents the dimensionless position within the droplet, with 0 and 1 corresponding to the center and surface of the droplet, respectively. Initially the solute concentration inside the droplet is uniform (C_0). However, solvent evaporation causes the solute concentration to increase at the droplet surface, forming a concentration gradient that results in solute diffusion toward the center of the particle. Computations are performed until the solute concentration at the droplet surface reaches the critical supersaturation (CSS). At this point, if the solute concentration at the droplet center ($r/R = 0$) is higher than the equilibrium concentration (ES), the solid phase will nucleate and grow throughout the entire particle, resulting in a dense sphere. On the other hand, if the

TABLE I. Physical properties of the $\text{ZrO}(\text{OH})\text{Cl}$ solution (20 °C).

Density (g/cm ³)	Viscosity (Pa s)	Heat capacity (J/(g K))	ES (mol/l)	CSS (mol/l)
1.14	0.012	4.184	5.7	8.0

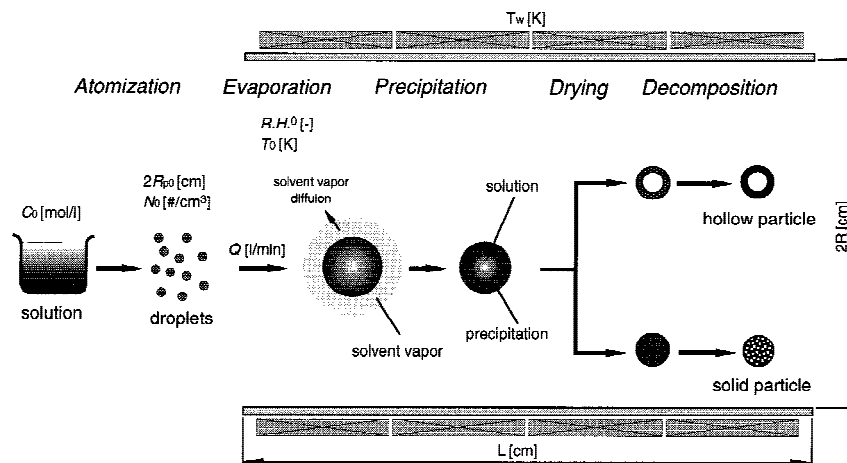


FIG. 3. Description of the simulation model.

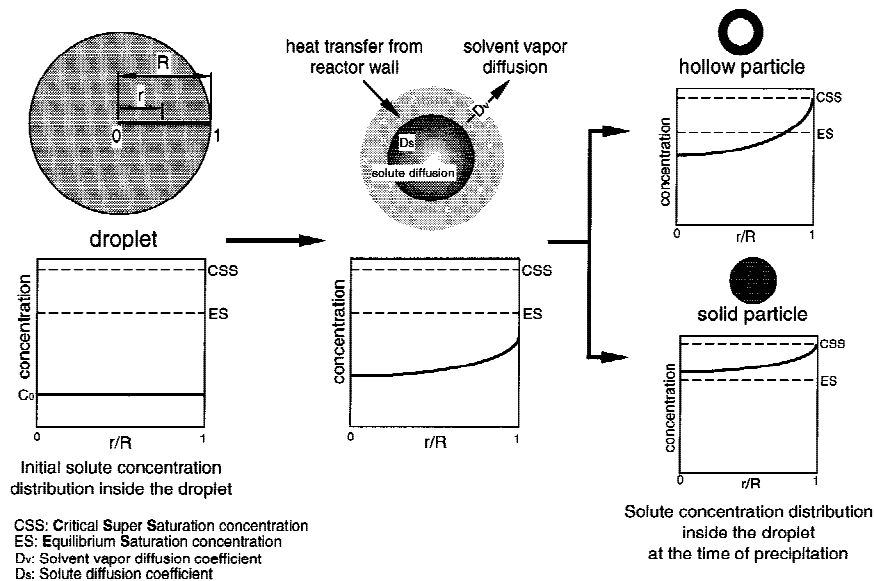


FIG. 4. Change of solute concentration distribution inside the droplet. CSS is the critical supersaturation concentration, and ES is the equilibrium concentration.

solute concentration at the center is lower than the ES, a hollow particle will form. The CSS and the ES values of aqueous solution of zirconium hydroxide chloride were referred to the values which Zhang and Messing¹⁴ has obtained experimentally (Table I).

To model this system, several assumptions were made: (i) The temperature within a droplet is uniform; however the temperature of both the gas and the droplets change due to solvent evaporation and heat transfer from the reactor walls. (ii) The effects of gravity and viscosity are negligible. (iii) The droplet maintains spherical shape, and the concentration fields within the droplet are spherically symmetric. (iv) Bubble formation or pressure buildup inside the droplet is absent, and the solid crusts formed are sufficiently permeable for solvent vapor dif-

fusion. (v) The flow is laminar and can be approximated as one-dimensional plug flow. (vi) The only mass transports occurring in the gas phase are solvent evaporation and vapor diffusion at steady state. (vii) The Kelvin effect is negligible because the final particle size is larger than 0.1 μm .¹⁶

At pseudo-steady state, the evaporation rate from a single droplet is given by

$$\frac{dm}{dt} = - \frac{4\pi R_p D_v M_g}{N_A} (n_s - n_g) \quad (1)$$

where m is mass of a droplet, R_p is the droplet radius, D_v is the diffusion coefficient of solvent vapor, N_A is the Avogadro constant, M_g is the

solvent molecular weight, and n_s and n_g are the vapor concentrations at the droplet surface and in the surrounding gas, respectively.

The rise in temperature of the droplet is given by the following equation derived from the heat transfer into the droplet gained from surrounding gas and the latent heat of solvent evaporation:

$$\frac{dT_s}{dt} = \frac{1}{mC_p} [4\pi R_p K(T_g - T_s)] + \lambda \frac{dm}{dt} \quad (2)$$

where T_s is the droplet temperature, T_g is the surrounding gas temperature, C_p is the droplet heat capacity, K is the thermal conductivity of the surrounding gas, and λ is the latent heat of solvent evaporation.

The transport equation describing the mass transfer/diffusion in the droplet was presented by Charlesworth and Marshall.⁷ As discussed previously, their formulation was difficult to solve numerically because of the moving boundary (solvent evaporation). Van der Lijn¹³ simplified the calculation by using dimensionless variable y as follows:

$$y = \frac{\int_0^r 4\pi r^2 M_s C(r) dr}{\int_0^R 4\pi r^2 M_s C(r) dr} \quad (3)$$

where M_s is the solute molecular weight and $C(r)$ is the solute concentration at a radius r . The denominator is the total mass of solute in the droplet, and the numerator is the mass of solute within a radius r . When $r = 0$, $y = 0$, and when $r = R_p$, $y = 1$. Therefore, even though R_p decreases with time due to droplet shrinkage, the value of y stays between 0 and 1.

In order to further simplify the diffusion equation, Jayanthi *et al.*¹¹ suggested that the dependent variable be changed from mass fraction of solute to u , which is the ratio of mass fraction of solvent W_{A1} to the mass fraction of solute,

$$u = \frac{1000\rho - M_s C(r)}{M_s C(r)} \quad (4)$$

Then using Eqs. (3) and (4), the diffusion equation becomes

$$\frac{\partial u}{\partial t} = \frac{16\pi^2}{z_0^2} \frac{\partial}{\partial y} \left[D_s \left\{ \frac{\rho_1^2}{(1+u)^2} \right\} r^4 \frac{\partial u}{\partial y} \right] \quad (5)$$

where ρ_1 is the droplet density and D_s is the solute diffusion coefficient.

The initial conditions for the diffusion equation are as follows:

$$u = \frac{1000\rho_1 - M_s C(R_{p0})}{M_s C(R_{p0})} \quad m = m_0 \quad R = R_{p0} \quad T_s = T_0 \quad (6)$$

where $C(R_{p0})$ is the solute concentration, m_0 is droplet mass, R_{p0} is droplet radius, and T_0 is the temperature of the droplet. Subscript 0 denotes the initial value. We assume that the initial droplet temperature is equal to the temperature of the carrier gas at the inlet.

The boundary conditions are as follows:

$$\frac{\partial u}{\partial y} = 0 \quad \text{at } y = 0 \quad (7)$$

$$\frac{4\pi R_p^2 \rho_1^2 D_s}{z_0(1+u)^2} \frac{\partial u}{\partial y} = \frac{dm}{dt} \frac{1}{4\pi R_p^2} \quad \text{at } y = 1 \quad (8)$$

By using the variables u and y , the droplet radius can be expressed as follows:

$$R_p^3 = \left[\frac{3z_0}{4\pi} \int_0^1 \frac{1+u}{\rho_1} dy \right] \quad (9)$$

As solvent evaporates from the droplets in the reactor, the vapor concentration of the carrier gas will increase. This increase is governed by (i) the solvent vapor introduced into the gas by droplet evaporation and (ii) vapor loss by diffusion from the gas to the reactor wall. The change in vapor concentration can be written as

$$\frac{dn_g}{dt} = -4\pi R_p D_v N_0 (n_g - n_s) - \frac{2K_m(n - n_w)}{R} \quad (10)$$

where n_g , n_s , and n_w are the vapor concentration in the surrounding gas, at the droplet surface, and at the reactor wall, respectively. R is the radius of the reactor tube, N_0 is the droplet number concentration, and K_m is the vapor mass transfer coefficient for laminar tube flow.

The temperature of the surrounding gas results from a balance between the heat transfer to droplets and from the reactor wall,

$$\frac{dT_g}{dx} = \frac{1}{FC_{pa}} [-4\pi^2 R^2 R_p^2 N_0 h_s (T_g - T_s) + 2\pi R h_w (T_w - T_g)] \left(\frac{dt}{dx} \right) \quad (11)$$

where x is the reactor axial coordinate, Q_m is the carrier gas molar flow rate, and C_{pa} is the heat capacity of the wet air. h_s and h_w are the heat-transfer coefficients at the droplet surface and at the reactor wall, respectively.

Assuming the carrier gas is ideal, the droplet residence time along the reactor can be found as follows:

$$\frac{dt}{dx} = \frac{0.06\pi R^2}{Q} \left(\frac{T_0}{T_g} \right) \frac{(1 - y_w)}{(1 - y_w^0)} \quad (12)$$

where t is the residence time, x is the reactor axial coordinate/length, Q is the carrier gas flow rate, T_g and T_0 are the temperature of carrier gas at the current position, x , and at the reactor inlet, $x = 0$, respectively, and

y_w and y_w^0 are the solvent mole fraction in the carrier gas at x and $x = 0$, respectively. The correction factor $(1 - y_w)/(1 - y_w^0)$ accounts for the change in the vapor content of the carrier gas as a result of droplet evaporation.

The temperature gradient along the hot wall reactor, dT_w/dx , was measured for the reactor used in the experiments, and T_w was expressed as a function of x -axis length, x . The wall of the reactor does not interact with the solvent, which corresponds to a no-flux condition at the wall. For more detailed information regarding the parameters and properties mentioned above, see Jayanthi *et al.*¹¹ and the appendix of Xiong and Kodas.¹²

The model allows the exploration of the influence of parameters such as the reactor temperature, the wall temperature gradient, the initial solution concentration, the initial droplet size, and the droplet number concentration on the final particle morphology. In addition, variables such as the droplet temperature and the solute concentration distribution within the droplet can be investigated as a function of distance along the reactor. The calculation procedure is as follows: (i) The values of m , T_g , u , R_p , n_g , T_g , and x are calculated at an interval of 10^{-3} s. New values of these variables are calculated from the previous values. These new values are used to calculate the time derivative. The calculations are stopped when the solute concentration at the droplet surface reaches the critical supersaturation concentration as determined in Eq. (5). (ii) Changes in mass, temperature, and radius for a single droplet are calculated using Eqs. (1), (2), and (9). The interior of the droplet is divided into 50 sections. The solute concentrations in each section are calculated using Eq. (5), and then the contribution from each section is summed to obtain the total solute concentration distribution inside the droplet. (iii) The changes in the vapor concentration and the temperature in the carrier gas due to interactions with the droplet population are calculated using Eqs. (10) and (11). The axial positions of droplets in reactor tube are calculated from Eq. (12).

Equations (1), (2), (5), and (10)–(12) are coupled ordinary differential equations and were solved simultaneously using an integration tool package EPISODE.¹⁷

IV. RESULTS AND DISCUSSION

Initial experiments were performed to investigate the influence of the reactor temperature on the crystalline phase and morphology of the zirconia particles. The particles were produced from a solution concentration of 2.0 mol/l and a flow rate of 2.0 l/min, at a number of isothermal reactor temperatures. Figure 5 shows the x-ray diffraction (XRD) patterns of the resulting particles. The peaks from the particles obtained at 200 °C show only a slight similarity to those in the zirconia phase, indicating that the reaction temperature was too low for

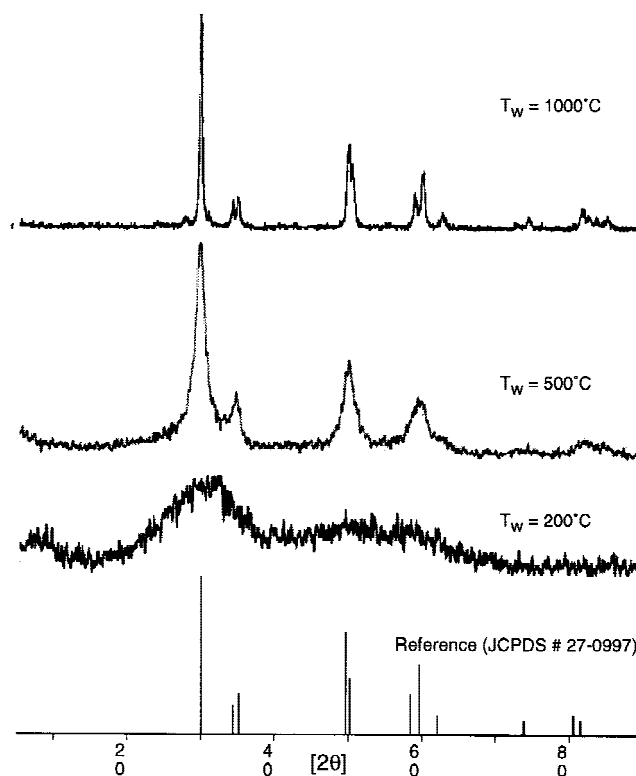


FIG. 5. XRD spectra of zirconia particles at different furnace temperatures (200, 500 °C). Other experiment conditions: $C_0 = 2$ mol/l; $Q = 2$ l/min.

the zirconia phase to be formed by thermal decomposition of the precursors. The XRD patterns of the particles prepared at 500 °C show excellent agreement with the reference spectrum (Powder Diffraction File JCPDS No. 27-0997) of ZrO_2 (tetragonal phase, metastable). When the process temperature is increased further (1000 °C), the ZrO_2 phase grew and the peaks become sharper. In this temperature, the XRD pattern included few peaks corresponding to monoclinic phase of zirconia.

Figure 6 shows pictures of the zirconia particles obtained by scanning electron microscopy (SEM). The figure shows that the particles formed at reactor temperatures of 100 and 200 °C were spherical and appear solid. However, at the higher temperatures of 300 and 500 °C, many of the particles were disrupted. This is particularly the case at 500 °C. This result indicates that at high temperatures, precipitation occurs only in the region around the particle surface, due to rapid solvent evaporation and slow solute diffusion.⁷ As solvent is depleted from the droplet surface, the temperature will rise substantially. Thermal diffusion is much larger than mass diffusion. Hence, the solvent could be trapped in the core of the droplet and heated to temperatures much above the normal boiling point. In fact, it is known that temperatures in multicomponent droplet vaporation can exceed the limit of superheat. In that case, nucleation of the liquid solvent

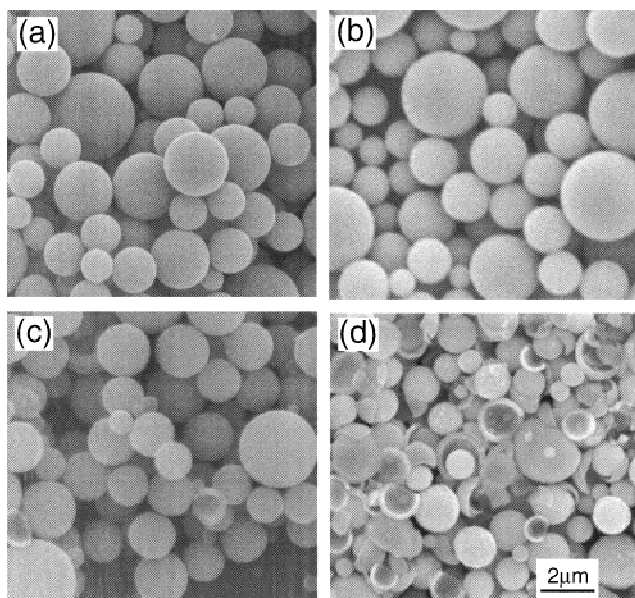


FIG. 6. Effect of furnace temperature on the morphology of zirconia particles: (a) 100 °C, (b) 200 °C, (c) 300 °C, and (d) 500 °C. Other experiment conditions: $C_0 = 2$ mol/l; $Q = 2$ l/min.

occurs with the formation of a gas bubble and subsequent disruption of the droplet. It is necessary to investigate further on these mechanisms.

Figure 7 shows results of model calculations for initial conditions of $2R_{p0} = 4.5$ μm , $N_0 = 5 \times 10^6$ cm^{-3} , $C_0 = 2.0$ mol/l, $\text{RH}^0 = 0\%$, and constant temperature distribution (see Fig. 8). Figure 7(a) shows the change of droplet diameter along the reactor axis at different reactor temperatures. Clearly solute precipitation occurred faster at higher reactor wall temperatures due to faster evaporation rates. Figure 7(b) shows the solute concentration distribution inside the droplet at the time of precipitation (i.e., when the solute concentration at the surface reaches the CSS). At reactor wall temperatures, T_w , of 100 and 200 °C, the solute concentration at the center is higher than the ES when the surface reaches the CSS. Thus, at these conditions the formation of solid particles is predicted. Conversely, at temperatures of 300 and 500 °C, $C_{(r=0)}$ is lower than the ES when $C_{(r=1)}$ reaches the CSS predicting hollow particle formation. This prediction agrees with the experimental results shown in Figs. 6(c) and 6(d), indicating good correlation between the numerical and experimental results.

To further explore the spray pyrolysis process, the effect of the temperature profile within the reactor on droplet evaporation and ultimate particle morphology was investigated. Figure 8 shows two different temperature profiles, constant and increasing, used in the present study. The temperature profiles were produced by adjusting the five heating zones. It is evident from the figure that the linearly increasing temperature profile will result in a lower heating rate along the reactor. Particles were

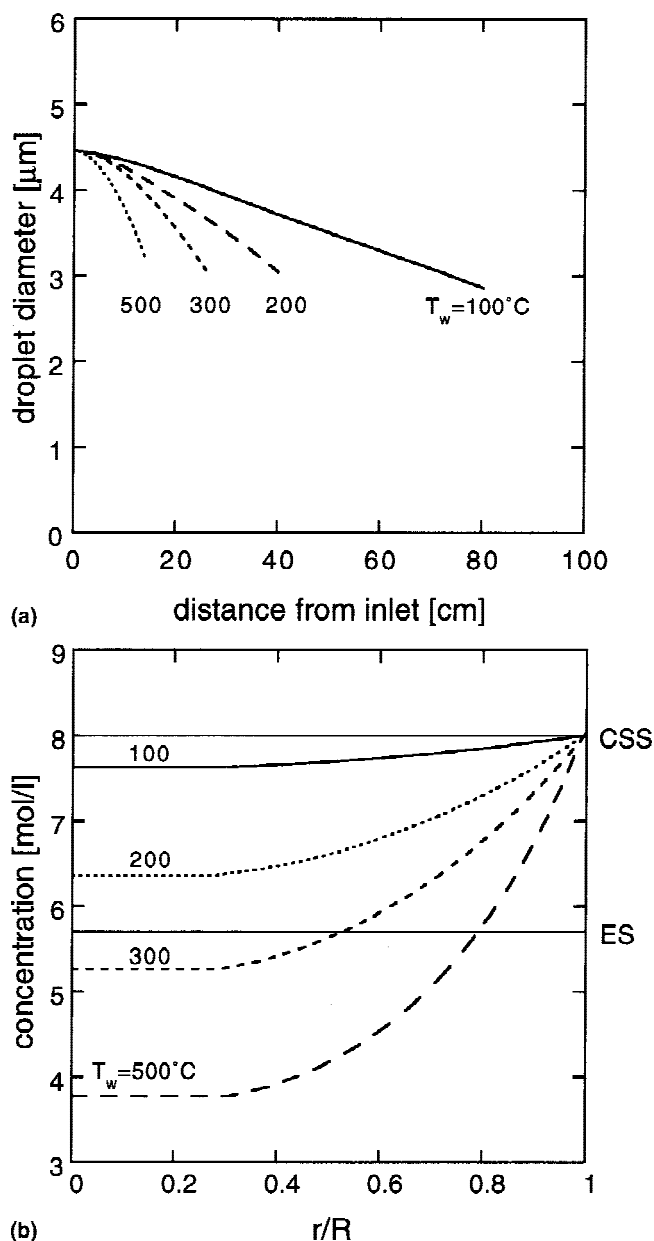


FIG. 7. Effect of furnace temperature on (a) the droplet/particle size and (b) the solute concentration distribution inside the droplet at the time of precipitation. Conditions: $D_{p0} = 4.5$ μm ; $C_0 = 2.0$ mol/l; $Q = 2.0$ l/min; $\text{RH}^0 = 0\%$.

produced using the two different profiles for several carrier gas flow rates resulting in a number of particle residence times and heating rates. SEM photographs of the resulting particles are shown in Fig. 9. The ZrO_2 particles produced at 500 °C and a flow rate of 2.0 l/min are disrupted and hollow. Changing to either an increasing temperature profile or a longer residence time has little effect on the final particle morphology. As seen in Fig. 9, both changes in the process are necessary to shift the morphology toward the production of more spherical particles with fewer disrupted particles.

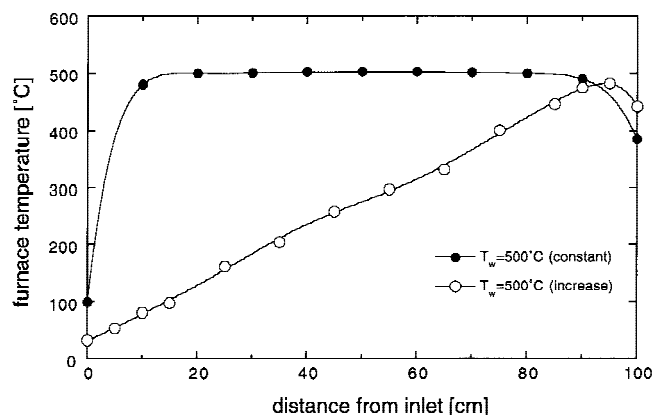


FIG. 8. Furnace wall temperature distribution.

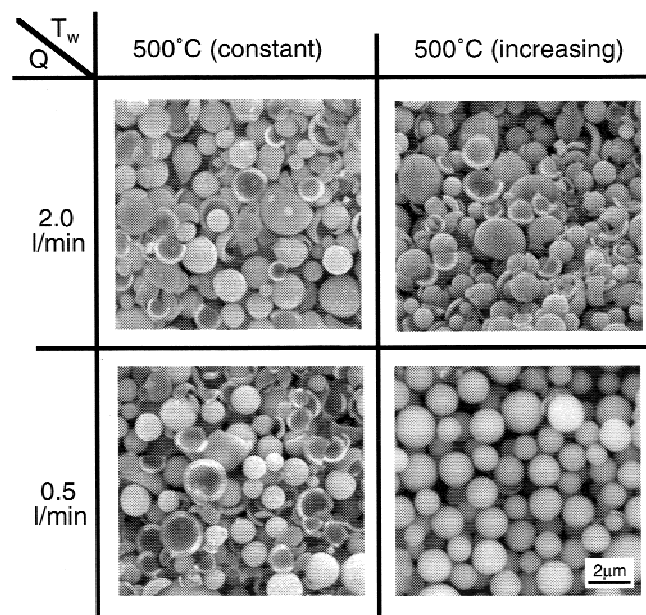
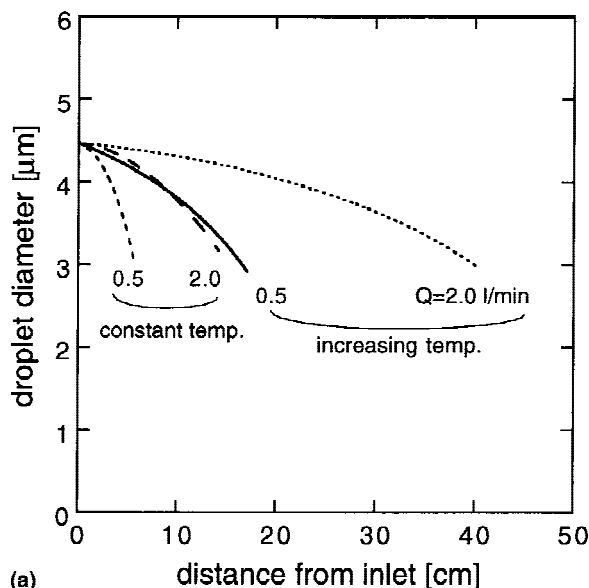
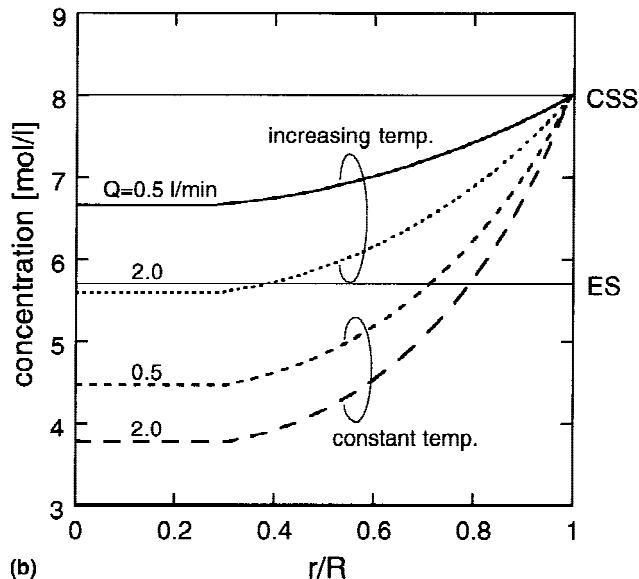


FIG. 9. Effect of temperature distribution and the residence time on morphology of zirconia particles. $C_0 = 2.0$ mol/l.

Figure 10 presents simulation results for the experimental conditions shown in Fig. 9. The use of the slowly increasing temperature profile gives lower evaporation rates than a constant profile for both flow rates. As a result, this operation decelerates the onset of solute precipitation [Fig. 10(a)] and reduces the formation of hollow, disrupted particles [Fig. 10(b)]. However, as seen in Fig. 9, it is necessary to both change the temperature profile and residence time to obtain solid particles at 500 °C. Neither change on its own slows evaporation rates enough for the center of the particle to reach the equilibrium saturation at the point at which solute nucleation occurs on the surface. A numerical simulation with an exceedingly low flow rate of 0.1 l/min at a constant temperature profile (500 °C) was also performed. The morphology of final particles is predicted to be solid.



(a)



(b)

FIG. 10. Effect of furnace temperature distribution and the carrier gas flow rate on (a) the droplet/particle size and (b) the solute concentration distribution inside the droplet at the time of precipitation. Conditions: $D_{p0} = 4.5$ μ m; $C_0 = 2.0$ mol/l; $RH^0 = 0\%$.

However, it is difficult to carry out an experiment with such a low flow rate of 0.1 l/min because the sprayed droplets cannot be transported well.

Figure 11 shows the simulation results of several different droplet number concentrations (N_0). It is clear from Fig. 11(a) that the smaller the number concentration of droplets, the faster the onset of precipitation, increasing the likelihood that hollow particles will form. For the conditions represented in Fig. 11, a droplet number concentration of 7.5×10^6 cm^{-3} should result in solid particles. However, when further increasing the number concentration to $N_0 = 2.0 \times 10^7$ cm^{-3} , the solution con-

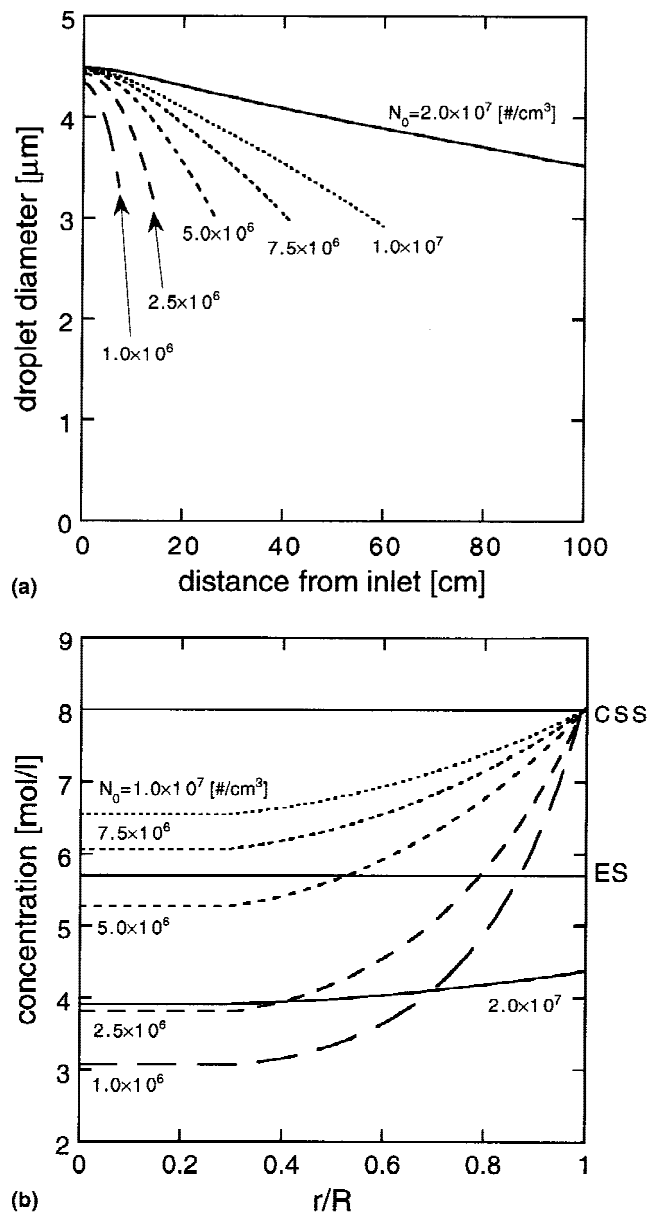


FIG. 11. Effect of droplet number concentration on (a) the particle size and (b) the solute concentration distribution inside the droplet. Conditions: $D_{p0} = 4.5 \mu\text{m}$; $T_w = 300 \text{ }^\circ\text{C}$; $Q = 2.0 \text{ l/min}$; $\text{RH}^0 = 0\%$.

centration at the surface does not reach the ES by the time the droplets exit the reactor, and precipitation will not occur. Clearly, an increase in the number concentration of droplets will result in more evaporation and a larger solvent vapor concentration in the carrier gas. As a result, the evaporation rate will decrease, delaying precipitation. Figure 11(a) also predicts that the final particle diameter will increase as the droplet number concentrations decrease. This increase is due to the fact that the hollow particles that form under the lower number concentration conditions have larger outer diameters.

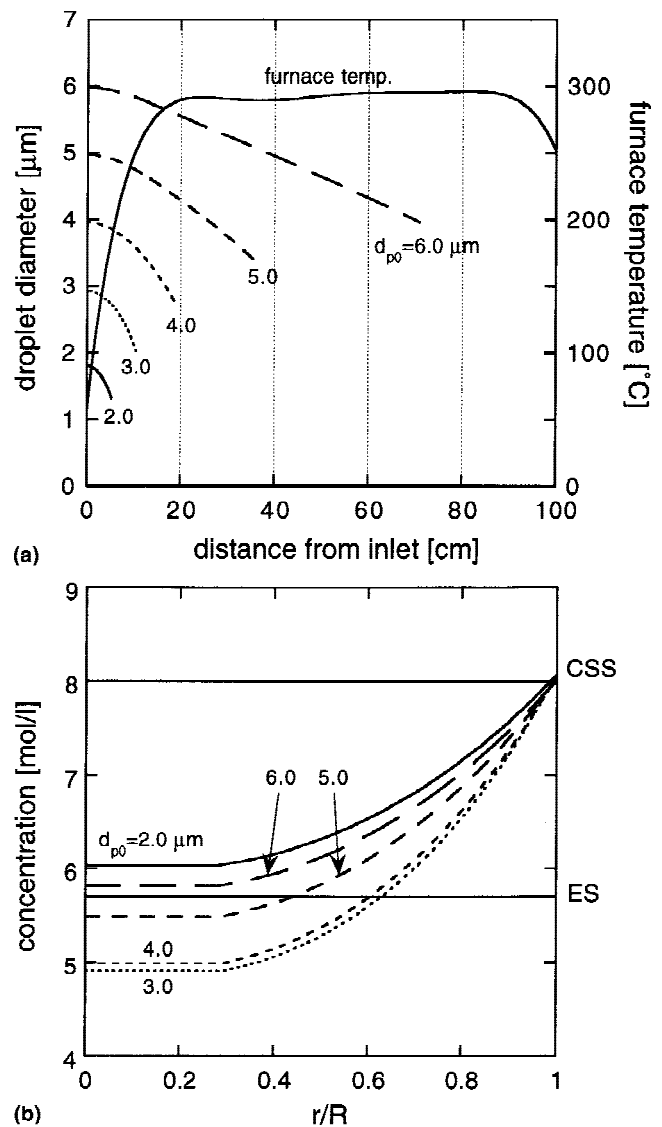


FIG. 12. Effect of initial droplet diameter on (a) the particle size and (b) the solute concentration distribution inside the droplet at the time of precipitation at the constant temperature distribution with $T_w = 300 \text{ }^\circ\text{C}$. Conditions: $C_0 = 2.0 \text{ mol/l}$; $Q = 2.0 \text{ l/min}$; $\text{RH}^0 = 0\%$.

Figure 12 shows simulation results for different initial droplet diameters at a wall temperature of 300 $^\circ\text{C}$ with a solution molality of 2.0 mol/l and a flow rate 2.0 l/min. The temperature distribution of the reactor is superimposed over the evolution of droplet diameters along the length of the reactor. As expected, the final particle diameter decreases as the diameter of the initial droplet decreases. It has been generally proposed that the use of smaller droplets in spray pyrolysis will produce solid particles because the diffusion distance for the solute is shorter, resulting in a more uniform concentration distribution within the particle. A previous theoretical study concluded that the initial droplet diameter does not affect the concentration profile inside the droplet at the time of

precipitation because the characteristic times for diffusion and evaporation depend in the same way on the particle radius.¹¹ However, contrary to these arguments, it is interesting to note that the formation of solid particles is predicted for $d_{p0} = 2$ and $6 \mu\text{m}$ and the hollow particles for $d_{p0} = 3, 4,$ or $5 \mu\text{m}$ [Fig. 12(b)]. As shown in Fig. 12(a), the reactor temperature increases rapidly from its initial temperature to the reactor wall temperature in the first 20 cm of the reactor. For small initial sizes, the majority of the evaporation and precipitation of the droplet are completed during this initial high-temperature gradient. The ultimate morphology of these particles is predicted to be hollow. On the other hand, for larger initial droplet sizes (e.g., $d_{p0} = 6 \mu\text{m}$), the majority of the particle evolution occurs during the isothermal region of the furnace, and the resulting particles are solid. In comparison to the smaller droplet, for $d_{p0} = 6 \mu\text{m}$ the heating rate is reduced and as a result the formed particles are solid. For $d_{p0} = 2 \mu\text{m}$, the temperature gradient is not as high as in the cases of $d_{p0} = 3$ or $4 \mu\text{m}$, so the final formed particles are solid. In the case of droplets having diameter larger than $6 \mu\text{m}$, the droplets exit 1-m length reactor without precipitation, because the solution concentration at the surface does not reach ES.

In order to confirm the relationship between temperature distribution along the reactor and the initial droplet diameter, the experiment was repeated using a linearly increasing temperature profile with a maximum temperature of $300 \text{ }^\circ\text{C}$. Figure 13 shows the simulation results for this profile, with the other parameters the same as Fig. 12. In the increasing temperature profile, the temperature of the reactor just reaches $300 \text{ }^\circ\text{C}$ before the exit of the reactor. A reduction in starting droplet diameter allows the formation of solid particles. From these results, it is clearly necessary to design a reactor to give an appropriate temperature distribution and residence time in order to produce particles with desirable morphology.

V. CONCLUSION

A spray pyrolysis model for fine particle preparation has been developed from a combination of two previous models. The model, for the first time, simultaneously considered the comparison of results obtained from experiment and numerical simulation. The results include the influence of operation parameters on the following: (i) changes of size and temperature of multiple droplets along a laminar reactor (ii) the solute concentration gradient inside the droplets (iii) the final morphology of prepared particles.

In general, the predicted simulation results are in good agreement with those obtained from the experiment. The solid particles can be formed if the reactor temperature is low or has a gradual distribution, the initial solute concentration is high, and the flow rate of carrier gas is low.

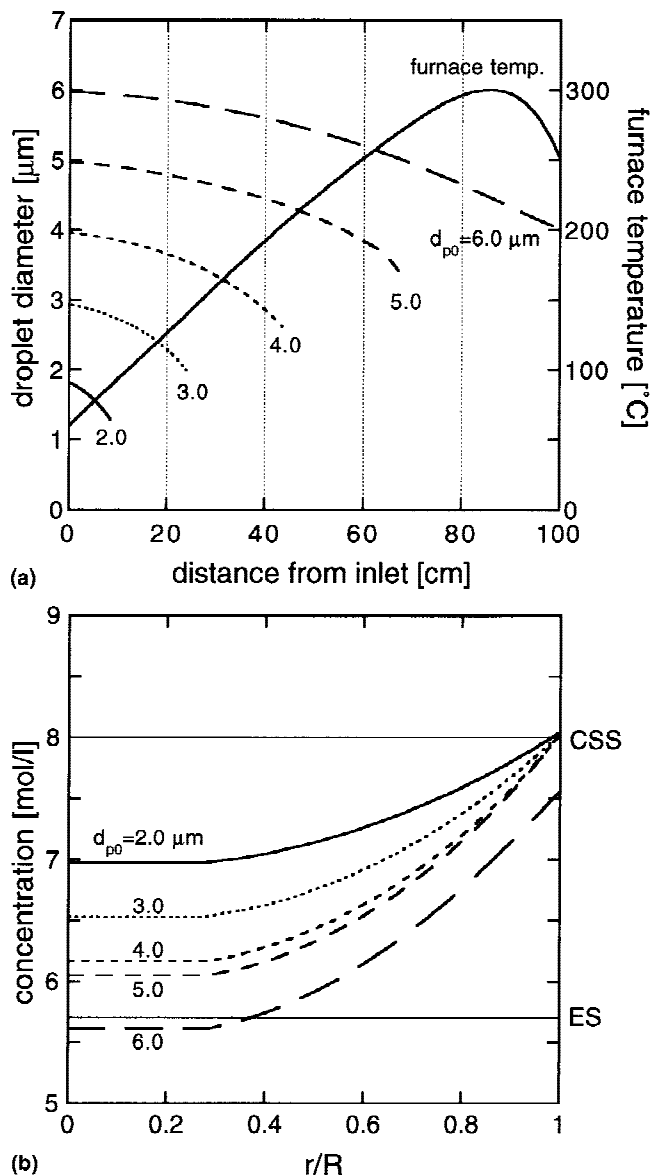


FIG. 13. Effect of the increasing temperature distribution on parameters that are the same as Fig. 12.

The simulation also indicates that the hollow particles in spray pyrolysis is formed if the initial droplets are large and the droplet number concentration is low. The model should be useful in solving some problems on the spray pyrolysis process; however, it is necessary to investigate further the determination of critical solution concentration and its temperature-dependent nucleation or crystal growth of the related materials.

ACKNOWLEDGMENTS

T. Komiya was very helpful in the experimental work. Support from the Ministry of Education, Culture, and Science of Japan (Grant No. 10650745) and the Hiroshima Industrial Technology Organization is gratefully

acknowledged. Nikkei-MEL (a joint venture between Nippon Light Metal Co. Ltd., Tokyo, Japan, and MEL Chemicals, Flemington, NJ) provided the precursor.

NOMENCLATURE

C_0	initial solution concentration	(mol/l)
C_{pa}	heat capacity of surrounding gas	(J/(mol K))
C_{pd}	heat capacity of droplet	(J/(mol K))
CSS	critical supersaturation concentration	(mol/l)
$C(r)$	solute concentration at a radius r	(mol/l)
d_{p0}	initial droplet diameter	(cm)
D_s	solute diffusion coefficient	(cm ² /s)
D_v	solvent vapor diffusion coefficients	(cm ² /s)
ES	equilibrium saturation concentration	(mol/l)
h_s	heat-transfer coefficient at the droplet surface	(J/cm ² s K)
h_w	heat-transfer coefficient at the reactor wall	(J/cm ² s K)
K	thermal conductivity of surrounding gas	(J/cm s K)
K_m	vapor mass transfer coefficient for laminar tube flow	(cm/s)
L	reactor length	(cm)
M_g	solvent molecular weight	(g/mol)
M_s	solute molecular weight	(g/mol)
m	droplet mass	(g)
m_0	initial droplet mass	(g)
N_0	vapor concentration at the droplet surface	(no./cm ³)
N_A	Avogadro constant	(No./mol)
n_g	vapor concentration in surrounding gas	(molecules/cm ³)
n_s	vapor concentration at the droplet surface	(molecules/cm ³)
n_w	vapor concentration at the reactor wall	(molecules/cm ³)
Q	carrier gas flow rate	(l/min)
Q_m	carrier gas molar flow rate	(mol/s)
R	reactor tube radius	(cm)
r	radial coordinate	(cm)
RH ⁰	relative humidity in surrounding gas	(-)
R_p	droplet radius	(cm)
R_{p0}	initial droplet radius	(cm)

t	time	(s)
T_0	initial temperature of reactor inlet	(K)
T_g	temperature of surrounding gas	(K)
T_s	temperature at the droplet surface	(K)
T_w	temperature at the reactor wall	(K)
u	ratio of mass fraction of solvent to mass fraction of solute	(-)
x	reactor axial coordinate	(cm)
y	ratio z to z_0	(-)
y_w	vapor mole fraction in surrounding gas	(-)
y_w^0	vapor mole fraction in surrounding gas at the reactor inlet	(-)
z	mass of solute present from the droplet center to a radius r	(g)
z_0	total mass of solute in the droplet	(g)
λ	latent heat of vaporization	(J/g)
ρ_1	density of the droplet	(g/cm ³)

REFERENCES

1. G.L. Messing, S.C. Zhang, and G.V. Jayanthi, *J. Am. Ceram. Soc.* **76**, 2707 (1993).
2. N. Tohge, M. Tatsumisago, T. Minami, K. Okuyama, M. Adachi, and Y. Kousaka, *J. Am. Ceram. Soc.* **74**, 2112 (1991).
3. K. Okuyama, I.W. Lenggoro, N. Tagami, S. Tamaki, and N. Tohge, *J. Mater. Sci.* **32**, 1229 (1997).
4. I.W. Lenggoro, Y.C. Kang, T. Komiya, K. Okuyama, and N. Tohge, *Jpn. J. Appl. Phys.* **37**, L288 (1998).
5. Y.C. Kang, S.B. Park, I.W. Lenggoro, and K. Okuyama, *J. Mater. Res.* **14**, 2611 (1999).
6. W.E. Ranz and W.R. Marshall, *Chem. Eng. Prog.* **48**, 141, 173 (1952).
7. D.H. Charlesworth and W.R. Marshall, Jr., *AIChE J.* **6**, 9 (1960).
8. Y. Sano and R.B. Keey, *Chem. Eng. Sci.* **27**, 881 (1982).
9. K.H. Leong, *J. Aerosol Sci.* **18**, 511 (1987).
10. H. Yu, *Part. Sci. Technol.* **13**, 149 (1995).
11. G.V. Jayanthi, S.C. Zhang, and G.L. Messing, *Aerosol Sci. Technol.* **19**, 478 (1993).
12. Y. Xiong and T.T. Kodas, *J. Aerosol Sci.* **24**, 893 (1993).
13. J. van der Lijn, *Agricultural Res. Report No. 845* (1976).
14. S.C. Zhang and G.L. Messing, in *Ceramic Powder Science III*, edited by G.L. Messing, S. Hirano, and H. Hausner (American Ceramic Society, Westerville, OH, 1990), p. 49.
15. M. Shimada, T. Seto, and K. Okuyama, *AIChE J.* **39**, 1859 (1993).
16. W.C. Hinds, *Aerosol Technology* (Wiley, New York, 1982).
17. A.C. Hindmarsh and G.D. Byrne, Lawrence Livermore National Laboratory Report, UCID-30112 (1977).